SOFT ROBOTS

A biosensing soft robot: Autonomous parsing of chemical signals through integrated organic and inorganic interfaces

Kyle B. Justus[1], Tess Hellebrekers[2], Daniel D. Lewis[3], Adam Wood[1], Christian Ingham[1], Carmel Majidi[1,2,4]*, Philip R. LeDuc[1,4]*, Cheemeng Tan[3]*

The integration of synthetic biology and soft robotics can fundamentally advance sensory, diagnostic, and therapeutic functionality of bioinspired machines. However, such integration is currently impeded by the lack of soft-matter architectures that interface synthetic cells with electronics and actuators for controlled stimulation and response during robotic operation. Here, we synthesized a soft gripper that uses engineered bacteria for detecting chemicals in the environment, a flexible light-emitting diode (LED) circuit for converting biological to electronic signals, and soft pneu-net actuators for converting the electronic signals to movement of the gripper. We show that the hybrid bio-LED-actuator module enabled the gripper to detect chemical signals by applying pressure and releasing the contents of a chemical-infused hydrogel. The biohybrid gripper used chemical sensing and feedback to make actionable decisions during a pick-and-place operation. This work opens previously unidentified avenues in soft materials, synthetic biology, and integrated interfacial robotic systems.

INTRODUCTION

The next generation of soft robotic systems will be tremendously enhanced by integrating synthetic biology and soft materials. Synthetic biology allows the development of bioinspired architectures that enable the integrated functionality of biological systems across different length scales. Such advancements complement recent progress in soft robotics, which uses soft materials to achieve compliant, lightweight, and multifunctional systems that match the robust mechanical properties and rich versatility of natural biological tissues and organisms (1–7). To date, the building blocks of these soft robots have largely been limited to material architectures composed of elastomers, fluids, metal alloys, and other inorganic matter. These include artificial muscle actuators that use pneumatics, shape memory alloy, dielectric elastomers, and a variety of other methods for robot limb motion (3) and artificial skin technologies that are capable of mechanically robust sensing and circuit wiring (2) and color change through microfluidics (8), chemical stimulation (9), or electroluminescence (10). At the systems level, soft and elastic materials have been used to create biologically inspired robots that mimic natural organisms (11–16) and bioinspired grippers (17, 18). Recently, there have been efforts to combine soft materials with natural cells to create "biohybrid" systems that respond to external stimuli. Examples include swimming and crawling biohybrid robots that are powered by contractile cells cultured on a polydimethylsiloxane (PDMS) substrate (19, 20) or a three-dimensional (3D) printed scaffold (21). By reprogramming the inner workings of cells to exploit their inherent versatility, researchers have also created microscale machines capable of functioning as sensors, computational tools, and timekeeping devices (22–27). The resulting synthetic biological systems allow for miniaturization of versatile chemical signal detection (28, 29). Together, these properties make synthetic cells promising candidates as subcomponents within an integrated, flexible, bioinspired structure for applications in soft robotics or wearables (30). The successful implementation of synthetic biological systems within flexible, soft robots has the potential to increase system functionality and reduce spatial requirements for external control systems.

A fundamental challenge in integrating cells with soft robots is the lack of an interfacial module for simultaneously achieving signal exchange between the external environment and cells, communication between the cells and internal electronics, and control between the internal electronics and host mechanics of the robot. Such an interfacial module would have to prevent the escape of the engineered cells while allowing for the exchange of chemical or electronic signals from the environment. Moreover, the module must be capable of converting these environmental signals to cellular signals and, last, to the electronic signals. All the signal conversion must be accomplished while the module remains compliant to the flexible movement of the robot and achieve the above functions within small-scale devices.

RESULTS

To demonstrate how these challenges can simultaneously be addressed, we designed and integrated a biosensing module featuring genetically engineered *Escherichia coli* into soft robotic grippers that contain embedded electronics and are capable of fluidic actuation (Fig. 1A). The basic module comprises a patterned elastomeric well that is sealed with a porous membrane to house a genetically engineered strain of *E. coli*. We selected *E. coli* as the chemical sensing layer because of the flexibility for incorporating a broad range of existing synthetic genetic circuits, the modularity of adding *E. coli* to the soft robots, and the ability to create a new class of soft robotic sensor modality (31, 32). This bacterial strain was designed to produce a genetic response to a widely used chemical inducer, isopropyl

[1]Department of Mechanical Engineering, Carnegie Mellon University, Pittsburgh, PA 15213, USA. [2]Robotics Institute, Carnegie Mellon University, Pittsburgh, PA 15213, USA. [3]Department of Biomedical Engineering, University of California, Davis, Davis, CA 95616, USA. [4]Departments of Biological Sciences, Computational Biology, and Biomedical Engineering, Carnegie Mellon University, Pittsburgh, PA 15213, USA.
*Corresponding author. Email: cmajidi@andrew.cmu.edu (C.M.); prl@andrew.cmu.edu (P.R.L.); cmtan@ucdavis.edu (C.T.)
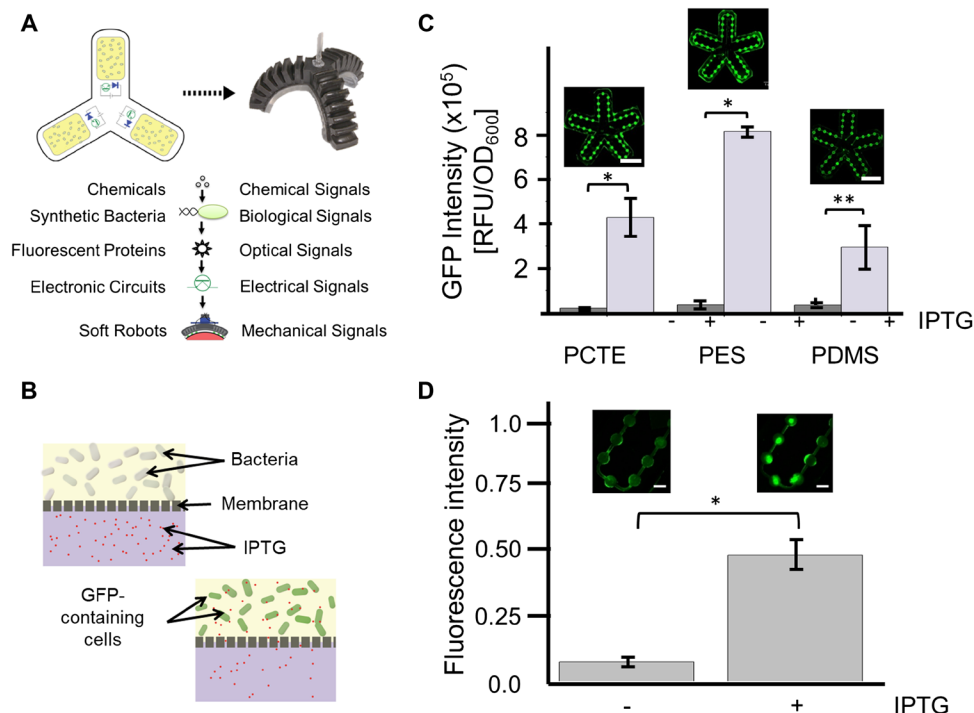
Fig. 1. Integrating chemical-responsive synthetic cells and flexible materials for a biosensing soft robot. (**A**) Our approach integrated genetically modified *E. coli* housed in fluidic wells and channels within a PDMS polymer mold. This approach enables an integrated soft robotic system featuring pneumatic actuation and embedded electronics with feedback from engineered cells. (**B**) The sealing membranes have pores that allowed chemical stimuli while rejecting bacteria to maintain biosensing capabilities. (**C**) To have control over the engineered cell interface, various membrane compositions were integrated with the device and evaluated for permeability, including PCTE, PES, and PDMS. Scale bars, 2 cm. The level of fluorescence expression due to IPTG permeation through each membrane [PCTE ($n = 3$), PES ($n = 4$), and PDMS ($n = 4$)] was measured using a plate reader. Data represent three to four replicates and SEM (*$P < 0.05$ and **$P < 0.10$). (**D**) Induced chemosensitive bacteria were introduced into a patterned PDMS layer sealed by a transparent PDMS membrane and imaged using a laser scanner to observe the fluorescent signal from within the device. Scale bars, 3 mm. Normalized data represent 10 measurements and SEM (*$P < 0.05$).

β-D-1-thiogalactopryanoside (IPTG), in the form of a fluorescent protein. The embedded electronic components then excite and detect the fluorescent protein before distributing the information to a central processing unit (CPU) to initiate robotic decision making and actuation. This integrated approach allows for truly autonomous robotic functionality in which grasping tasks are performed following decisions based on external stimuli that are detected and photonically transmitted by embedded synthetic cells.

Biosensing module

Before demonstrating the full soft biohybrid robot implementation, we first established the integration of the cells within the soft material carrier medium used for the robot housing. We controlled the interface between the external environment and the hybrid bio–light-emitting diode (LED)–actuator module that allowed for chemical diffusion and prevented the escape of the bacteria while maintaining the flexibility of the soft robot. We examined three membrane compositions— polyethersulfone (PES) and polycarbonate track-etched (PCTE) membranes (*33*) and a porous PDMS-NaHCO₃ membrane—by inducing cells housed within the sealed elastomeric wells (*34*). The PES and PCTE membranes provided more uniform pore sizes and distributions, but they lacked elastomeric properties and optical transparency—properties that were achieved with the PDMS-based membrane. All membranes have pore sizes less than 0.5 μm in diameter, which enabled the retention of *E. coli* bacteria while

allowing the transport of chemical stimuli into the device from the external environment (Fig. 1B). These membranes retained the bacteria in the patterned wells of the PDMS biolayer. The permeability of each membrane was measured using IPTG-sensitive bacteria and fluorescence microspheres as controls to examine the effectiveness of each membrane (Fig. 1C). All three membrane materials demonstrated the diffusion of fluorescent dye into the device wells, supporting all three as viable components within the device design. Because of the position of the membrane relative to the pneu-net actuators, PES and PCTE membranes could be used in this device despite lacking elastomeric properties because they were located in the strain-limiting layer and were not required to stretch during gripper motion.

Beneath the membranes that allow the exchange of chemicals, we incorporated a flexible PDMS layer using 3D printed molds for housing synthetic bacteria. The wells and channels within this layer were then sealed with the membrane, and synthetic bacteria were delivered through the liquid media via fluidic channels. Next, we examined the patterned well geometries regarding growth and optical performance using bacteria that carried a chemically inducible *pIV_GFP* genetic module (*35*) that expressed a green fluorescent protein (GFP). The growth of the genetically engineered bacteria in four distinct geometries of constant volume (circular, rhombic, square, and ellipsoidal patterns) were measured and found to produce minimal effects on bacterial proliferation (figs. S1 and S2). Furthermore, log-phase bacteria were induced with IPTG, introduced into the

embedded wells, and then cultured for at least 4 hours. The resulting GFP intensities of the synthetic bacteria yielded about 500% increase in normalized fluorescence (Fig. 1D).

LED integration

Embedded electronics were required to transmit signals from the cell (e.g., fluorescent signaling) to the soft robot CPU and controller. Both the membrane and the cell chamber constituted the biolayer that allowed the bacteria to detect and respond to chemicals in the environments. To convert the biological signal to an electronic signal, we implemented an onboard and centimeter-scale circuit to convert fluorescence signals from bacteria to electrical signals. The output fluorescence of the bacteria required both an excitation wavelength and emission detector. Therefore, we validated that onboard LEDs were sufficient to excite fluorescent proteins and then introduced a photodetector to measure the output fluorescence.

To accomplish this, we embedded LEDs within the elastomer substrate of the biolayer as an excitation light source. The LEDs were powered by an off-board supply and arranged radially in the direction of the five flexible appendages comprising the soft gripper design. The bottom of the biolayer was bonded to a silicone elastomer (Ecoflex 00-30, Smooth-On Inc.) embedded within a network of inflatable air chambers (Materials and Methods and fig. S3). Next, the biolayer was filled with IPTG-induced *E. coli* that have synthesized GFP. The GFP within the wells was then excited by the embedded LED circuit near the excitation peak and observed using a series of glass filters and a wide-field stereomicroscope (Fig. 2A, LED circuit removed from composite in image processing; raw images in Materials and Methods and figs. S4 and S5). Induced cells within the system produced a fluorescence expression level of about 400% of uninduced and unmodified *E. coli* (Fig. 2B, Materials and Methods, and fig. S4). We also show that the light source could activate an optogenetic circuit of bacteria that carried a *pDusk_GFP* genetic module, which expresses GFP in the absence of blue light (470 nm) (figs. S6 to S8) (*36*). The results together suggest that the onboard light source could excite fluorescent proteins or modulate the conformation of a light-responsive protein, which was further demonstrated by repressing the gene expression using the module itself (fig. S9).

FlexPCB integration

After building an interface between cell response and electronic signaling, we next integrated these cell electronic responses into a functional soft robotic system. Building upon the excitation light source, we developed a soft electronic circuit that detected the fluorescence signals and converted it into a usable electronic signal with which to guide robotic behavior through an end effector. To achieve the onboard detection module, we embedded a flexible printed circuit board (FlexPCB) within the biolayer (Materials and Methods and fig. S10). The circuit placed an LED and phototransistor directly below each cell chamber. A critical design challenge involved maximizing LED brightness while avoiding phototransistor saturation. In addition, the LED wavelength must sufficiently activate the fluorescent proteins with a complementary filter for the phototransistor that has a wavelength between the excitation and emission spectrum of the cell's fluorescent output. The final design used mCherry fluorescent proteins ($\lambda_{excitation} = 587$ nm and $\lambda_{emission} = 610$ nm), an amber LED ($\lambda_{peak} = 574$ nm), a red filter ($\lambda_{pass} > 590$ nm), and a phototransistor ($\lambda_{max} = 570$ nm). We embedded the circuit into a strain-limiting PDMS layer, submerged the device in controlled aqueous solutions for
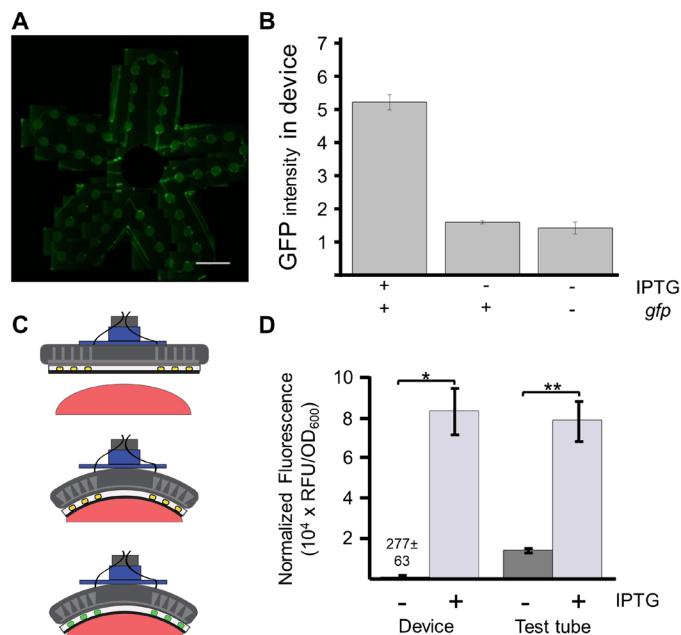
Fig. 2. Establish the organic-inorganic interface of the gripper. (**A**) The synthetic bacteria were introduced into individual wells containing induced synthetic *E. coli*. The excitation capabilities of the embedded blue wavelength LED circuit were tested using a stereomicroscope and a combination of filters for wide-field imaging, demonstrating the capabilities of the LED circuit to elicit a response from the contained cells. Scale bar, 10 mm. (**B**) Housed within the device, induced bacteria exhibited higher fluorescence intensities than uninduced and unmodified *E. coli*. Data represent nine measurements and SEM (*$P < 0.01$ and **$P < 0.01$). (**C**) The sensing capabilities of the device were evaluated in an aqueous environment, and chemosensitive cells were used to determine the presence of IPTG in submerged hydrogels. (**D**) The device successfully distinguished between IPTG-infused and standard hydrogels, producing a higher normalized florescence ratio between the test and control than the same strains induced in test tubes. Data represent means ± SEM for three separate experiments (*$P < 0.05$ and **$P < 0.05$).

chemical sensitivity conditions, and collected the phototransistor data. With this optimal balance of wavelength sensitivity and filtering, we show that this onboard circuit could differentiate between IPTG$^+$ from control environments. Together, we demonstrate the detection of a genetic response and subsequent conversion into a usable electrical signal within a flexible soft robotic architecture.

Soft gripper actuation

Although the hybrid bio-LED-actuator module allowed us to control the biological response, the module should not interfere with the natural mechanical compliance of the host soft robot. We measured the actuation of the soft gripper with the modified biolayer and observed that the liquid media and bacteria were retained within the wells despite the deformation (Materials and Methods and fig. S11). On the basis of our design configuration, the wells and bacteria were placed with the strain-limiting layer of the actuator, which was required for the pneu-net to bend in a preferential direction. Along with active control of the soft robotics platform, it was also essential to demonstrate environmental sensing functionality of the integrated cellular module (movie S1). We examined the response of our designed sensing approach using a molded hydrogel infused with the chemical stimulus IPTG while submerged in a water bath (Fig. 2C). The device was suspended via pneumatic tubing within an incubator

at 30°C and slowly lowered until the center of the device contacted the hydrogel. Next, the pressure in the pneu-net channels was increased to initiate contact between the membrane-sealed surface of the device and the submerged hydrogel. After the contact, the relative fluorescence intensities of the device interacting with an IPTG hydrogel were almost 300 times higher than negative controls lacking IPTG, performing similar to the bacteria in test tubes (Fig. 2D). The results indicate that the chemosensing bacteria within the device were integrated to respond to environmental cues from external environments within our soft robotic system.

Integrated soft robot gripper

Combining our advances, we demonstrated a soft robotic decision-making system that detects and responds to an environmental chemical signal. To accomplish this, we combined the biolayer, FlexPCB, and pneu-nets to create a biogripper that was mounted to a 4-DOF robotic arm, where it could interact with an incubated media bath (Fig. 3, A and B; Materials and Methods; and figs. S12 and S13). The circuit sampled the fluorescent output of the cells and stored the data. The robot arm was programmed to raise the device during the sampling period and lower the biogripper into the bath between samples to avoid reflective noise from the bath. After the sampling, the device could detect the genetic response induced by the presence of IPTG (Fig. 3C and fig. S10 and S14). We used these results to calibrate a threshold-based control program for a pick-and-place scenario. Depending on the voltage trend collected during the experiment, the system reacted based on our programmed modules:

If the bath was found to contain IPTG, then the object was not deployed and the operator was alerted; if the bath was found not to contain IPTG, then the arm picked up the object and placed it into the bath (Fig. 3D and movie S2).

DISCUSSION

We have successfully implemented an embedded biosensing module within a soft robotic testbed capable of using genetically engineered cells to detect and respond to external chemical stimuli and then detecting the genetic response to inform robotic behavior. By integrating synthetic bacteria into a soft robotic system, we demonstrate the ability to expand the functionality of flexible devices through the utilization of existing biological architectures. The inclusion of synthetic bacteria as sensing mechanisms exploits the inherent abilities of cellular level biological systems to respond to a variety of stimuli at a low spatial cost. The combination of fluidic channels and wells with microfilter membranes allows for the retention of sensory bacteria, as well as the interaction between the synthetic cells and both chemical and optical cues. Along with broader materials selection, this fluidic functionality allows for a versatile and flexible device capable of engaging and responding to foreign objects in an aqueous environment.

Our purpose in adopting a multistep approach to sensing was to demonstrate that it is possible to combine synthetic biology, flexible electronics, and soft robotic actuation into a single integrated architecture. We selected IPTG and engineered *E. coli* because their properties
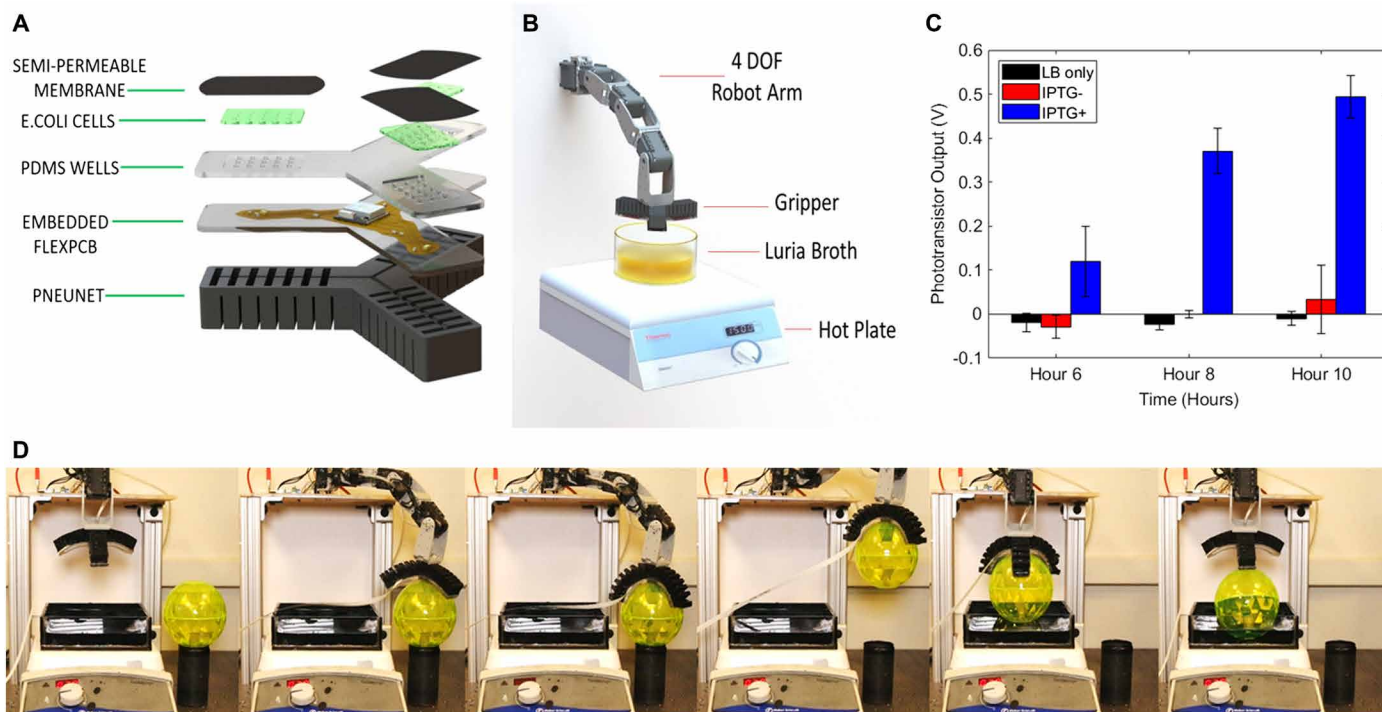
Fig. 3. Robotic sorting using a soft biosensing gripper. (**A**) The components of the biosensing soft gripper featured FlexPCB and embedded phototransistors in addition to the previously tested components. (**B**) The setup featured an incubated media bath, into which the gripper was submerged via a 4-DOF robotic arm to test for sensing modality for chemical inducers. (**C**) Phototransistor output over time for IPTG$^+$ bath with cells in the device varied significantly over time in comparison to control cases, allowing the system to make decisions based on the genetic response of the cells. Errors bars represent SE, and each data point represent an average of three experiments. $P < 0.05$ for IPTG$^+$ bath with cells against both groups. (**D**) The soft robot sorted an object based on the phototransistor signal using the three-finger biogripper to deploy the object into a bath after classifying the bath as IPTG.

and interactions are well understood in the existing context of synthetic biology. In this respect, they were intended to function as a model system (or surrogate) for a much wider range of chemo-biophotonic processes that may enable future applications. More generally, they demonstrate the ability to broaden the scope of soft robotic sensing to include novel biohybrid modalities that are possible with synthetic biology.

Future efforts will extend this work by creating stable hybrid organic-inorganic systems, akin to the coexistence of the microbiome in the human body. Such systems will incorporate soft robotic biosensing into human-compatible soft machines and expand the complexity of signal processing by the synthetic cells. The working temperature range of this device is largely dependent on the cells, which performed best from 30° to 42°C. In addition, the system's response time, lifetime, and storage time were limited and these parameters are expected to improve alongside research to optimize these parameters in synthetic biology. Moreover, further progress in synthetic biology will enable a wider range of chemical sensing modalities and the use of synthetic pathways that use protein-based networks (31).

MATERIALS AND METHODS

Biological components

The *E. coli* BL21(DE3) was used to create z-competent cells before transformation. The plasmid *pIV_GFP* was created in a previous work (27) and inserted into cells to allow for synthesis of GFP. This plasmid was designed to initiate transcription of the *gfp* gene in the presence of the chemical stimulus IPTG.

Constructing optogenetic plasmid

To construct a plasmid capable of changing gene expression in response to blue light, we digested the pDusk plasmid (Addgene 43795) with Sal I and Not I, ligated in a polymerase chain reaction fragment containing GFP, and transformed the assembled vector into TOP10 cells. Variants of pDusk_GFP, pDusk_v37_GFP, and pDusk_v38_GFP were made by changing the ribosome binding site. The ribosome binding site was manipulated by annealing two short single-stranded DNA oligomers together to form an insert with a new RBS, then phosphorylating the insert, and ligating the insert with the vector at the Xba I and Sal I sites.

Growth rate detection

The growth rate of the bacteria within the device was measured through a Beckman Coulter DU730 ultraviolet (UV)–visible spectrophotometer (Beckman Coulter, Brea, CA, USA). Optical density measurements at 600-nm wavelength were recorded before the introduction of the bacteria to the device and after subsequent growth in an incubated shaker (37°C).

Protein expression measurement

The fluorescence intensity of reporter proteins was measured using a Tecan Infinite M1000 plate reader (Tecan, Männedorf, Switzerland). Fluorescence intensities were normalized by optical density measurements to obtain average intensity per cells.

Culture well fabrication

The culture wells were created using a negative plastic master mold via 3D printing (Stratasys, Eden Prairie, MN) due to the deep feature depths, which are more difficult to achieve with traditional photolithography approaches. Desired molds were produced using SolidWorks (Dassault Systèmes SolidWorks Corporation, Waltham, MA) and imported to the Objet printing setup, where the molds were then formed with VeroWhite printing material. The molds were then baked at 60°C for 4 hours to remove residue solvents, which can inhibit the curing of PDMS. PDMS was mixed at a 10:1 base-to-curing agent ratio and poured into the 3D printed master molds before desiccation for 45 min. The PDMS-filled molds were then transferred to an oven at 60°C for at least 2 hours until fully cured. Last, the PDMS layers were removed from the mold using an X-ACTO knife, and excess PDMS was removed.

Electronics integration

An LED circuit was designed featuring three or five LEDs (depending on the gripper configuration), with a peak wavelength of 465 nm and gull wing leads (Kingbright, City of Industry, CA) all arranged in series in a compact, circular pattern. The LEDs were soldered together and connected to a copper wire lead to which an external DC power supply was connected. Once the circuit was completed, it was placed centrally within uncured PDMS deposited in the 3D printed negative mold of the fluidic channels and culture wells.

Porous membrane fabrication

Through a similar work by Jiao *et al.* (34), porous PDMS membranes were created via in situ reaction. The Sylgard 184 curing agent was mixed with sodium bicarbonate powder at a 1:1 mass ratio and mixed thoroughly before setting for 1 hour. The two materials were mixed once again before mixing with the Sylgard 184 base agent at a 1:5 mass ratio and desiccating for 20 min. The prepolymer sodium bicarbonate mixture was then deposited on 120°C heat release tape at a thickness of 100 μm via a thin-film applicator. The PDMS was then cured at 60°C in an oven for at least 2 hours. The cured membranes were then submerged in a bath of 13 M HCl and Triton X-100 (100× dilution) for 1 hour before being thoroughly washed with water and allowed to dry in an oven at 60°C (2 to 4 hours).

Device assembly

The device was composed of two main layers, one containing the biological components and the other housing the electronic components. First, 25 g of PDMS prepolymer was poured into a negative mold, having the features of the fluidic channels and bacterial growth wells. A series of blue wavelength LEDs were then placed in the center of the PDMS layer and allowed to partially cure on a hot plate. Once partially cured (25 min at 70°C on a hot plate), a fully cured EcoFlex layer having pneumatic channels (achieved through 3D printed negative mold) was placed on top of the PDMS layer and allowed to adhere and seal off the interior channels. After this curing process, the PDMS-EcoFlex device was carefully removed from the fluidic channel mold, and the biolayer interface was then sealed off with a microfilter membrane (PDMS-NaHCO$_3$, PCTE, or PES) via plasma oxidation. PCTE and PES membranes were purchased from Sterlitech with pore sizes of 0.2 μm (PCTE and PES) and 0.4 μm (PCTE). PES membranes were adhered to the PDMS biolayer component via a 3-aminopropyltriethoxysilane (APTES) pretreatment process outlined by Aran *et al.* (33), and the PCTE membranes were adhered using a combination of an APTES approach and sealing the membrane edges using PDMS prepolymer before curing to prevent delamination.

Permeability

Permeability of the membrane to IPTG was measured using multiple methods to verify molecular transport through the transmembrane pores. As an initial validation, membranes were suspended across microchannels (500 µm width), which were formed as PDMS negative molds from 3D printed masters, and sealed using plasma oxidation. After sterilization with 70% ethanol and UV radiation, fluorescent beads (1 µm in diameter) in Luria broth (LB) media were introduced into the upper channel, whereas sterile LB media was flowed into the lower channel, separated by the membrane. The two fluids were left to sit statically in the channels for 2 hours before fluorescent measurements using a plate reader were performed and compared with initial fluorescent readings of each solution.

Stereomicroscopy

A digital charge-coupled device camera (The Imaging Source Europe, GmbH) mounted on a stereomicroscope (SZX12, Olympus Corp., Waltham, MA) was used to perform wide-field imaging of the device to create a composite view of the LED excitation of GFP-producing cells housed within the PDMS layers. Imaging was performed with ×1 magnification with 18 V of power supplied to the five gull wing LEDs, whereas the sealed biolayer was positioned on an actuating stage and moved accordingly during a time series capture with 3-s intervals.

Pneumatic actuation

Deflection of the device through pneumatic action within the EcoFlex layer was measured using open-source motion-tracking software (Tracker). Pressure was increased within the channel manually with a syringe pump, and pressure levels were monitored using a piezoelectric pressure sensor (Honeywell, Morristown, NJ) interfaced with a microcontroller and MATLAB (Mathworks, Natick, MA). Pressure was increased in 0.5-psi increments from 0 to 5 psig. Positions were recorded along the pneumatic appendage in 0.5-cm increments for each pressure step.

Hydrogel preparation

Gelatin molds were prepared by mixing 15% (w/v) of gelatin from porcine skin (Sigma-Aldrich, St. Louis, MO) and heated to 80°C on a hot plate. Test samples were mixed with 1 µM IPTG (Sigma-Aldrich) before being left to cool in the plastic mold.

Hydrogel sensing test

Overnight cultures of bacteria were prepared in 3-ml volumes of LB with 1 µl of stock ampicillin (50 µg/ml) before placing on a shaker table at 37°C for 16 hours. The overnight cultures were then diluted 100× into fresh media and antibiotics and allowed to grow on the incubated shaker table for 4 hours. The bacteria were then extracted from the test tube and injected into the fluidic reservoirs of two devices. The remaining bacteria were then split into 1-ml volumes in fresh test tubes, one of which was induced with IPTG (1 mM). The two devices were placed in incubators at 30°C. One was brought into contact with an IPTG-infused gelatin mold submerged in LB, whereas the other was brought into contact with a standard gelatin mold submerged in LB. The pneu-net channels of the devices were activated in parallel using syringes and tubing fixed within a quick clamp to insure constant pressure. The devices were left in place for 4 hours before extraction via syringe. The samples were then measured using an absorbance and fluorescence plate reader (Tecan, Männedorf, Switzerland) along with the samples from the test tubes.

Plate reader comparison

Table S1 compares the phototransistor output, in volts, with the relative fluorescence unit output for the mCherry genetic constructs in BL21DE3 cells, dimensionless, from the fluorescence plate reader (Tecan, Männedorf, Switzerland). The cells were tested under mCherry conditions with an excitation frequency of 587 nm and an emission frequency of 610 nm.

SUPPLEMENTARY MATERIALS

robotics.sciencemag.org/cgi/content/full/4/31/eaax0765/DC1
Fig. S1. Growth curves of pT7 strains in varying well shapes more than 8 hours.
Fig. S2. Fluorescence images of induced pIV_GFP strains in varying well geometries.
Fig. S3. Schematic of the device fabrication.
Fig. S4. Wide-field imaging of induced GFP synthesis within the device.
Fig. S5. Method used to determine relative fluorescent intensities.
Fig. S6. Schematic representation of genetic modules.
Fig. S7. Fluorescence measurements of *gfp* strains after IPTG induction and incubation for 4 hours.
Fig. S8. Repression of gene expression in pDusk strains using blue light.
Fig. S9. Repression of gene expression in pDusk strains via embedded LEDs within the module.
Fig. S10. FlexPCB circuit design.
Fig. S11. Tracking software used to determine deflections of the actuated device.
Fig. S12. System architecture for sample-and-sort demonstration of the biosensing soft robotic capabilities.
Fig. S13. Cyberphysical architecture of the soft robotic system.
Fig. S14. Device fabrication with FlexPCB layer.
Table S1. Plate reader comparison.
Movie S1. Combining soft robotic modalities and fluorescence output for tactile sensing in hydrogels.
Movie S2. Detection of chemical inducers in a liquid bath and directed robotic sorting.

REFERENCES AND NOTES

1. S. Bauer, S. Bauer-Gogonea, I. Graz, M. Kaltenbrunner, C. Keplinger, R. Schwödiauer, 25th anniversary article: A soft future: From robots and sensor skin to energy harvesters. *Adv. Mater.* **26**, 149–161 (2014).
2. M. L. Hammock, A. Chortos, B. C.-K. Tee, J. B. H. Tok, Z. A. Bao, 25th anniversary article: The evolution of electronic skin (e-skin): A brief history, design considerations, and recent progress. *Adv. Mater.* **25**, 5997–6038 (2013).
3. F. Ilievski, A. D. Mazzeo, R. F. Shepherd, X. Chen, G. M. Whitesides, Soft robotics for chemists. *Angew. Chem. Int. Ed. Engl.* **50**, 1890–1895 (2011).
4. S. Kim, C. Laschi, B. Trimmer, Soft robotics: A bioinspired evolution in robotics. *Trends Biotechnol.* **31**, 287–294 (2013).
5. S. I. Rich, R. J. Wood, C. Majidi, Untethered soft robotics. *Nat. Electron.* **1**, 102–112 (2018).
6. D. Rus, M. T. Tolley, Design, fabrication and control of soft robots. *Nature* **521**, 467–475 (2015).
7. M. Wehner, R. L. Truby, D. J. Fitzgerald, B. Mosadegh, G. M. Whitesides, J. A. Lewis, R. J. Wood, An integrated design and fabrication strategy for entirely soft, autonomous robots. *Nature* **536**, 451–455 (2016).
8. S. A. Morin, R. F. Shepherd, S. W. Kwok, A. A. Stokes, A. Nemiroski, G. M. Whitesides, Camouflage and Display for Soft Machines. *Science* **337**, 828–832 (2012).
9. G. R. Gossweiler, C. L. Brown, G. B. Hewage, E. Sapiro-Gheiler, W. J. Trautman, G. W. Welshofer, S. L. Craig, Mechanochemically active soft robots. *ACS Appl. Mater. Interfaces* **7**, 22431–22435 (2015).
10. C. Larson, B. Peele, S. Li, S. Robinson, M. Totaro, L. Beccai, B. Mazzolai, R. Shepherd, Highly stretchable electroluminescent skin for optical signaling and tactile sensing. *Science* **351**, 1071–1074 (2016).
11. M. Calisti, M. Giorelli, G. Levy, B. Mazzolai, B. Hochner, C. Laschi, P. Dario, An octopus-bioinspired solution to movement and manipulation for soft robots. *Bioinspir. Biomim.* **6**, 036002 (2011).
12. M. Cianchetti, M. Calisti, L. Margheri, M. Kuba, C. Laschi, Bioinspired locomotion and grasping in water: The soft eight-arm OCTOPUS robot. *Bioinspir. Biomim.* **10**, 035003 (2015).
13. H.-T. Lin, G. G. Leisk, B. Trimmer, GoQBot: A caterpillar-inspired soft-bodied rolling robot. *Bioinspir. Biomim.* **6**, 026007 (2011).
14. R. V. Martinez, J. L. Branch, C. R. Fish, L. Jin, R. F. Shepherd, R. M. D. Nunes, Z. Suo, G. M. Whitesides, Robotic tentacles with three-dimensional mobility based on flexible elastomers. *Adv. Mater.* **25**, 205–212 (2013).

15. K. Suzumori, S. Endo, T. Kanda, N. Kato, H. Suzuki, A bending pneumatic rubber actuator realizing soft-bodied manta swimming robot. in *Proceedings of the IEEE International Conference of Robotics and Automation (ICRA)* (2007), pp. 4975–4980.

16. C. L. Zhou, K. H. Low, Design and locomotion control of a biomimetic underwater vehicle with fin propulsion. *IEEE ASME Trans. Mechatron.* **17**, 25–35 (2012).

17. R. Deimel, O. Brock, A novel type of compliant and underactuated robotic hand for dexterous grasping. *Int. J. Robot. Res.* **35**, 161–185 (2016).

18. X. Zhou, C. Majidi, O. M. O'Reilly, Soft hands: An analysis of some gripping mechanisms in soft robot design. *Int. J. Solids Struct.* **64-65**, 155–165 (2015).

19. A. W. Feinberg, A. Feigel, S. S. Shevkoplyas, S. Sheehy, G. M. Whitesides, K. K. Parker, Muscular thin films for building actuators and powering devices. *Science* **317**, 1366–1370 (2007).

20. J. C. Nawroth, H. Lee, A. W. Feinberg, C. M. Ripplinger, M. L. McCain, A. Grosberg, J. O. Dabiri, K. K. Parker, A tissue-engineered jellyfish with biomimetic propulsion. *Nat. Biotechnol.* **30**, 792–797 (2012).

21. C. Cvetkovic, R. Raman, V. Chan, B. J. Williams, M. Tolish, P. Bajaj, M. S. Sakar, H. H. Asada, M. T. A. Saif, R. Bashir, Three-dimensionally printed biological machines powered by skeletal muscle. *Proc. Natl. Acad. Sci. U.S.A.* **111**, 10125–10130 (2014).

22. T. L. Deans, A. Singh, M. Gibson, J. H. Elisseeff, Regulating synthetic gene networks in 3D materials. *Proc. Natl. Acad. Sci. U.S.A.* **109**, 15217–15222 (2012).

23. Y. Ding, F. Wu, C. Tan, Synthetic biology: A bridge between artificial and natural cells. *Life* **4**, 1092–1116 (2014).

24. M. B. Elowitz, S. Leibler, A synthetic oscillatory network of transcriptional regulators. *Nature* **403**, 335–338 (2000).

25. A. S. Khalil, J. J. Collins, Synthetic biology: Applications come of age. *Nat. Rev. Genet.* **11**, 367–379 (2010).

26. C. M. Tan, S.-J. Lo, P. R. LeDuc, C.-M. Cheng, Frontiers of optofluidics in synthetic biology. *Lab Chip* **12**, 3654–3665 (2012).

27. C. M. Tan, S. Saurabh, M. P. Bruchez, R. Schwartz, P. LeDuc, Molecular crowding shapes gene expression in synthetic cellular nanosystems. *Nat. Nanotechnol.* **8**, 602–608 (2013).

28. S. Slomovic, K. Pardee, J. J. Collins, Synthetic biology devices for in vitro and in vivo diagnostics. *Proc. Natl. Acad. Sci. U.S.A.* **112**, 14429–14435 (2015).

29. M. A. TerAvest, C. M. Ajo-Franklin, Transforming exoelectrogens for biotechnology using synthetic biology. *Biotechnol. Bioeng.* **113**, 687–697 (2016).

30. X. Liu, T.-C. Tang, E. Tham, H. Yuk, S. Lin, T. K. Lu, X. Zhao, Stretchable living materials and devices with hydrogel–elastomer hybrids hosting programmed cells. *Proc. Natl. Acad. Sci. U.S.A.* **114**, 2200–2205 (2017).

31. X. J. Gao, L. S. Chong, M. S. Kim, M. B. Elowitz, Programmable protein circuits in living cells. *Science* **361**, 1252–1258 (2018).

32. N. Ishii, K. Nakahigashi, T. Baba, M. Robert, T. Soga, A. Kanai, T. Hirasawa, M. Naba, K. Hirai, A. Hoque, P. Y. Ho, Y. Kakazu, K. Sugawara, S. Igarashi, S. Harada, T. Masuda, N. Sugiyama, T. Togashi, M. Hasegawa, Y. Takai, K. Yugi, K. Arakawa, N. Iwata, Y. Toya, Y. Nakayama, T. Nishioka, K. Shimizu, H. Mori, M. Tomita, Multiple high-throughput analyses monitor the response of *E. coli* to perturbations. *Science* **316**, 593–597 (2007).

33. K. Aran, L. A. Sasso, N. Kamdar, J. D. Zahn, Irreversible, direct bonding of nanoporous polymer membranes to PDMS or glass microdevices. *Lab Chip* **10**, 548–552 (2010).

34. K. X. Jiao, C. L. Graham, J. Wolff, R. G. Iyer, P. Kohli, Modulating molecular and nanoparticle transport in flexible polydimethylsiloxane membranes. *J. Memb. Sci.* **401–402**, 25–32 (2012).

35. M. I. Lebedeva, E. V. Rogozhkina, N. A. Tsyba, S. V. Mashko, A new T7 RNA polymerase-driven expression system induced via thermoamplification of a recombinant plasmid carrying a T7 promoter-Escherichia coli lac operator. *Gene* **142**, 61–66 (1994).

36. R. Ohlendorf, R. R. Vidavski, A. Eldar, K. Moffat, A. Moglich, From dusk till dawn: One-plasmid systems for light-regulated gene expression. *J. Mol. Biol.* **416**, 534–542 (2012).

Citation: K. B. Justus, T. Hellebrekers, D. D. Lewis, A. Wood, C. Ingham, C. Majidi, P. R. LeDuc, C. Tan, A biosensing soft robot: Autonomous parsing of chemical signals through integrated organic and inorganic interfaces. *Sci. Robot.* **4**, eaax0765 (2019).

Science Robotics

A biosensing soft robot: Autonomous parsing of chemical signals through integrated organic and inorganic interfaces

Kyle B. Justus, Tess Hellebrekers, Daniel D. Lewis, Adam Wood, Christian Ingham, Carmel Majidi, Philip R. LeDuc and Cheemeng Tan

ARTICLE TOOLS	http://robotics.sciencemag.org/content/4/31/eaax0765
SUPPLEMENTARY MATERIALS	http://robotics.sciencemag.org/content/suppl/2019/06/24/4.31.eaax0765.DC1
REFERENCES	This article cites 35 articles, 9 of which you can access for free http://robotics.sciencemag.org/content/4/31/eaax0765#BIBL
PERMISSIONS	http://www.sciencemag.org/help/reprints-and-permissions

Use of this article is subject to the Terms of Service